Molecular Sieving of Ethane from Ethylene through the Molecular Cross-Section Size Differentiation in Gallate-based Metal–Organic Frameworks

Zongbi Bao, Jiawei Wang, Zhiguo Zhang, Huabin Xing, Qiwei Yang, Yiwen Yang, Hui Wu, Rajamani Krishna, Wei Zhou,* Banglin Chen,* and Qilong Ren*

Abstract: *Purification of C_2H_4 from an C_2H_4/C_2H_6 mixture, one of the most important while challenging industrial separation processes, is mainly through energy-intensive cryogenic distillation. Now a family of gallate-based metal–organic framework (MOF) materials is presented, M-gallate (M = Ni, Mg, Co), featuring 3D interconnected zigzag channels, the aperture sizes of which (3.47–3.69 Å) are ideally suitable for molecular sieving of ethylene ($3.28 \times 4.18 \times 4.84$ Å^3) and ethane ($3.81 \times 4.08 \times 4.82$ Å^3) through molecular cross-section size differentiation. Co-gallate shows an unprecedented IAST selectivity of 52 for C_2H_4 over C_2H_6 with a C_2H_4 uptake of 3.37 mmol g^{-1} at 298 K and 1 bar, outperforming the state-of-the-art MOF material NOTT-300. Direct breakthrough experiments with equimolar C_2H_4/C_2H_6 mixtures confirmed that M-gallate is highly selective for ethylene. The adsorption structure and mechanism of ethylene in the M-gallate was further studied through neutron diffraction experiments.*

Olefin/paraffin separations are industrially critical processes, providing various primary feedstocks for the industrial manufacture of a variety of products, particularly household plastics.[1] Their separations have been recognized as one of the seven chemical separations to change the world because the total energy used for ethylene and propylene separation alone accounts for more than 0.3% of the global energy consumption.[2] Due to the similar sizes and volatilities of the molecules, industrial separation of ethylene from ethane currently relies on energy-intensive cryogenic distillation at high pressures (up to 22 bar) and temperatures as low as −25°C.[3] Tremendous energies could be saved if materials enabling the efficient separation of ethylene/ethane at ambient temperature and pressure were developed.

For this purpose, tremendous efforts have been devoted to investigate a great number of separation agents, such as membranes,[4] organic solvent-based absorbents,[5] and porous solid adsorbents.[6] Principally, adsorptive separation based on porous solid materials is a prospective and economically viable alternative to the energy-intensive distillation process. To develop adsorbents which preferentially adsorb ethane is of a practically significant interest for the separation of ethylene/ethane mixture, but the adsorption selectivity ever reported for ethane over ethylene is still not high enough.[7] Nowadays, one of the most popular adsorption-based separations of ethane and ethylene in porous materials was based on selective π-complexation interaction between ethylene and transition metals such as Ag$^+$/Cu$^+$ ions supported on alumina, resins, and zeolites.[8] However, ethylene is strongly bound and difficult to recover from these composite adsorbents. The complexation with metals may also lead to highly unstable and explosive products. Besides, some metal–organic frameworks (MOFs) with open metal sites (OMSs) rendered similar π-complexation towards ethylene molecules.[9] For instance, the series of MMOF-74 (M = Mg, Co, Ni, Mn, Fe) materials are an archetypal example with high-density OMSs, and perform well for the ethylene/ethane separation owing to a side-on coordination of the carbon–carbon double bond to the metal centers.[10] However, simultaneous co-adsorption of ethane resulted from polarization of OMSs in MMOF-74 is unavoidable, making it difficult to obtain high-purity ethylene at low cost of regeneration energy.

Ideal porous materials for gas separation are those with suitable pore sizes and geometries for size or shape sieving, only taking up smaller molecules while blocking the larger ones. Fortunately, ultra-fine tuning of the topology of the aperture could be readily accomplished in MOFs via ligand and/or metal ion substitutions,[11] as well in some zeolites.[6,8b,12] Benefitting from their highly ordered and well-defined pore structures, and adjustable pore dimensions, MOFs have attracted considerable attention as porous solid adsorbents in the field of gas storage and separation during the last two decades.[13] Among some of the pioneering works, molecular exclusion of methane and nitrogen from carbon

[*] Dr. Z. B. Bao, Dr. J. W. Wang, Prof. Z. G. Zhang, Prof. H. B. Xing,
    Dr. Q. W. Yang, Prof. Y. W. Yang, Prof. Q. L. Ren
    Key Laboratory of Biomass Chemical Engineering of Ministry of
    Education, College of Chemical and Biological Engineering
    Zhejiang University
    Hangzhou 310027 (P. R. China)
    E-mail: renql@zju.edu.cn

    Prof. B. L. Chen
    Department Department of Chemistry
    University of Texas at San Antonio
    One UTSA Circle, San Antonio, TX 78249-0698 (USA)
    E-mail: banglin.chen@utsa.edu

    Dr. H. Wu, Prof. W. Zhou
    NIST Center for Neutron Research
    National Institute of Standards and Technology
    Gaithersburg, MD 20899-6102 (USA)
    E-mail: wzhou@nist.gov

    Prof. R. Krishna
    Van't Hoff Institute for Molecular Sciences, University of Amsterdam
    Science Park 904, 1098 XH Amsterdam (The Netherlands)

    Supporting information and the ORCID identification number(s) for
    the author(s) of this article can be found under:
    https://doi.org/10.1002/anie.201808716.

dioxide,[14] ethylene, and carbon dioxide from acetylene,[15] propane from propylene,[16] branched paraffins from normal paraffins[17] have been successfully achieved by fine tuning of the MOF structures. However, it remains an ongoing challenge to seek out a porous solid material with suitable pore size and window shape to achieve the molecular sieving of ethylene and ethane with high enough efficiency.[8b]

Previously, the studies aimed at molecular sieving mainly focused on the difference between the kinetic diameters of gas adsorbates and the pore size of the adsorbent, and few insights into the complete molecular sieving through their van der Waals molecular dimension differentiation were obtained. Herein, we reported a family of MOF materials whose pore windows are ideally suitable for molecular sieving of ethylene and ethane through molecular cross-section size differentiation. The gallate-based MOFs feature three-dimensionally interconnected zigzag channels (3.47×4.85, 3.56×4.84, 3.69×4.95 $Å^2$ for Ni, Mg, Co-gallate, respectively). From the kinetic diameter point of view, it seems impossible for both ethylene (with the kinetic diameter of 4.163 Å) and ethane (4.443 Å) to get into the pore channels.[18] On the contrary, the appropriate aperture size is theoretically perfect for the separation of ethane ($3.81 \times 4.08 \times 4.82$ $Å^3$) and ethylene ($3.28 \times 4.18 \times 4.84$ $Å^3$)[19] (Supporting Information, Figure S1) considering that the aperture size is slightly larger than the minimum cross-section size of ethylene molecule (3.28×4.18 $Å^2$) but obviously smaller than that of ethane (3.81×4.08 $Å^2$; Figure 1c; Supporting Information, Fig-

ure S2). This means that ethane molecules could be excluded from the pore channels while ethylene molecules could enter the pore. Our hypothesis was indeed verified by adsorption isotherms and breakthrough experiments on M-gallate. The adsorption structure and mechanism of ethylene in the zigzag channels was further studied through neutron diffraction experiments. Our results show that M-gallate is a new benchmark porous material for adsorptive separation of ethylene and ethane.

The gallate-based MOFs, M-gallate ($M(C_7O_5H_4) \cdot 2H_2O$, M = Ni, Mg, Co), were prepared from the reaction of gallic acid and metal salts. The crystal structure of Ni-gallate was resolved by single-crystal X-ray diffraction analysis, and the structure of Mg, Co-gallate were inferred from the powder X-ray diffraction data thanks to the excellent crystallinity. Structure resolution revealed that the as-synthesized M-gallate are isostructural and crystallized in the $P3_221$ space group (Supporting Information, Table S1), in agreement with the previous report.[20] The framework structure is composed of infinite chains of corner-sharing distorted MO_6 octahedra connected through the organic ligands (four O atoms from the phenolic hydroxy groups of two different ligands, and two O from the carboxyl groups of another two ligands). The regular main channels are formed by spiral extension of the connection of metal octahedra and organic ligands around the c axis, along with regular branched channels leaning against the main ones (Figure 1a,b). Moreover, M-gallate shows the ideal quasi-discrete fusiform branched channels as
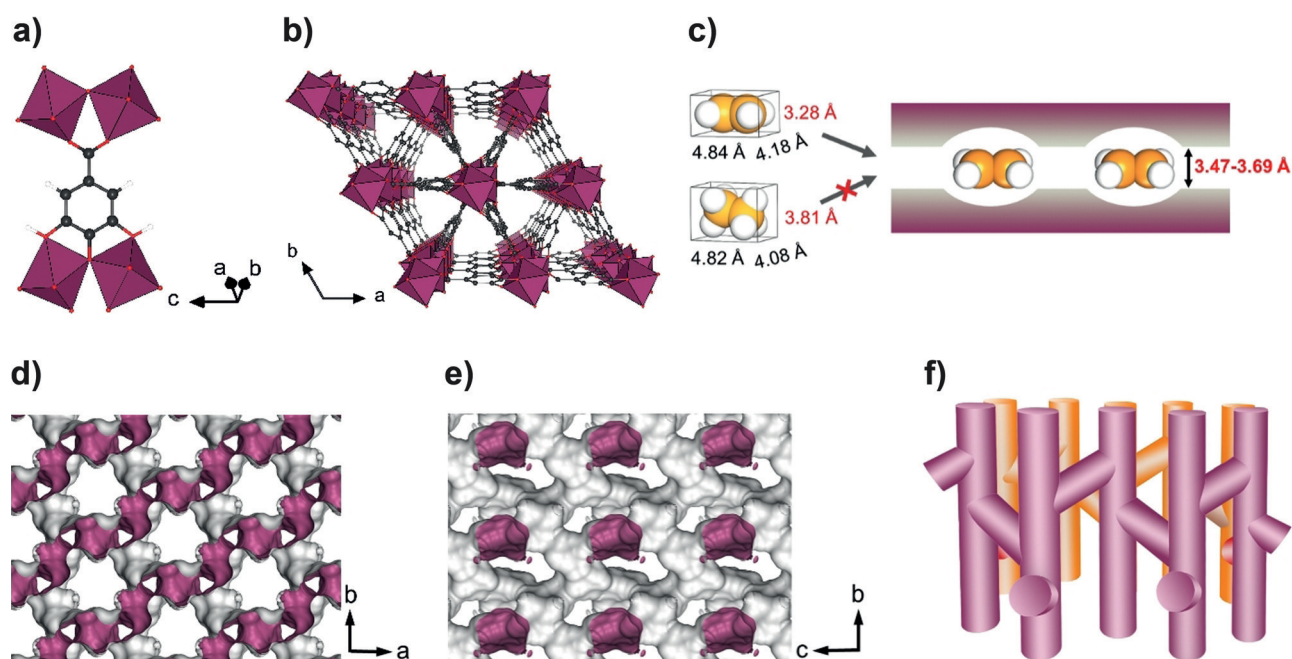
Figure 1. a) The coordination environment of gallate ligand and MO_6. M purple, C black, O red, H white. b) Perspective view of the structure along the c axis showing the triangular main channels and the regular branched channels leaning against the main ones. The H atoms are omitted for clarity. c) Diagram of the fusiform branched channels. Only ethylene can favorably enter the cavity because the limiting aperture size of M-gallate (3.47×4.85 $Å^2$ for Ni-gallate, 3.56×4.84 $Å^2$ for Mg-gallate, and 3.69×4.95 $Å^2$ for Co-gallate) matches well with the smallest cross-section size of C_2H_4 (3.28×4.18 $Å^2$), but is smaller than that of C_2H_6 (3.81×4.08 $Å^2$). The C atoms in C_2H_4 and C_2H_6 are particularly presented in orange. d),e) Accessible Connolly surface calculated with a Connolly radius of 1.0 Å. The quasi-discrete cavities of the fusiform branched channels are restrained by the narrow pore windows. f) Diagram of the zigzag channels. The zigzag channels in different layers are colored by purple and orange, respectively.

molecular sieves, where the larger cavities are interconnected by very narrow windows (Figure 1 d,e; Supporting Information, Figure S2). The interlaced zigzag channels are fully empty after the guest molecule removed (Figure 1 f), and the crystal lattice of M-gallate becomes slightly distorted with symmetry changing from the $P3_221$ to $P3_1$ space group (Supporting Information, Figure S3 and Table S2). The pore size still matches well with the smallest cross-section size of ethylene and remains smaller than that of ethane.

The permanent porosity of M-gallate was confirmed by adsorption isotherms of CO_2 at 195 K (Supporting Information, Figure S4) with Brunauer–Emmett–Teller (BET) surface areas estimated to be 424, 559, and 475 $m^2 g^{-1}$ for Ni, Mg, Co-gallate, respectively. Based on the encouraging microporous porosity characteristics, the separation potential for C_2H_4/C_2H_6 mixture was first examined by single-component equilibrium adsorption isotherms. As shown in Figure 2 a and the Supporting Information, Figures S5–S7, satisfactory C_2H_4 adsorption capacity is achieved on all M-gallates. Specially, Co-gallate exhibits the highest C_2H_4 uptake of 3.37 mmol g^{-1} at 298 K and 1 bar. As a very important parameter in industrial adsorptive separation process, the volumetric uptake of C_2H_4 on Co-gallate reaches up to 5.18 mmol mL^{-1},

surpassing most state-of-the-art performers, including the benchmark MOF material NOTT-300 (4.90 mmol mL^{-1}), next only to the family of MMOF-74 (Figure 2 c; Supporting Information, Table S3). It implies the high productivity of ethylene in the industrial adsorption process. It is worth noting that all M-gallate are capable of preventing C_2H_6 from entering the channels as evident with a low uptake (less than 0.31 mmol g^{-1}) at 298 K up to 1 bar. It is dramatically lower than those of best-performing porous materials, including zeolite 13X, NOTT-300 and the family of MOF-74 (Supporting Information, Table S3). Therefore, our adsorption findings confirmed that M-gallate is capable of efficiently blocking the slightly larger ethane molecules on the premise of high ethylene uptake.

In light of molecular exclusion of ethane, M-gallate show remarkable ideal adsorbed solution theory (IAST) selectivity for the equimolar C_2H_4/C_2H_6 mixture (Figure 2 b). Particularly, Co-gallate exhibits an unprecedented adsorption selectivity of 52 at 298 K and 1 bar, outperforming all MOF-based adsorbents ever reported, and setting up a new benchmark for the C_2H_4/C_2H_6 separation (Figure 2 b,c). To further confirm such outstanding separation performance of M-gallate for ethylene/ethane mixture, we also investigated the experimental breakthrough tests for C_2H_4/C_2H_6 (50/50, *v/v*) mixture. Figure 2 d shows the dimensionless concentration of C_2H_4/C_2H_6 exiting the adsorber packed with M-gallate as a function of the time at 1 bar. Complete separation was realized by all M-gallate, whereby C_2H_6 broke through very soon because of low uptake capacity; nevertheless, the signal of C_2H_4 was not detected longer than 55 min, denoting that pure C_2H_6 could be obtained until C_2H_4 was eluted. On the other hand, the bound C_2H_4 molecules in the column can be easily desorbed by an inert gas (helium) purge or the vacuum swing method after adsorption saturation to obtain high-purity C_2H_4 due to relatively weak interaction between C_2H_4 and M-gallate. As an important parameter to evaluate the strength of interaction between the adsorbent and the adsorbate, the isosteric heat of adsorption (Q_{st}) of C_2H_4 was calculated using the Clausius–Clapeyron equation. The obtained Q_{st} value at zero-coverage was 32, 39, 44 kJ mol^{-1} for Ni, Mg, Co-gallate (Supporting Information, Figure S8 and Table S3), which is remarkably lower than those of π-complexation-based MOF-74 with open
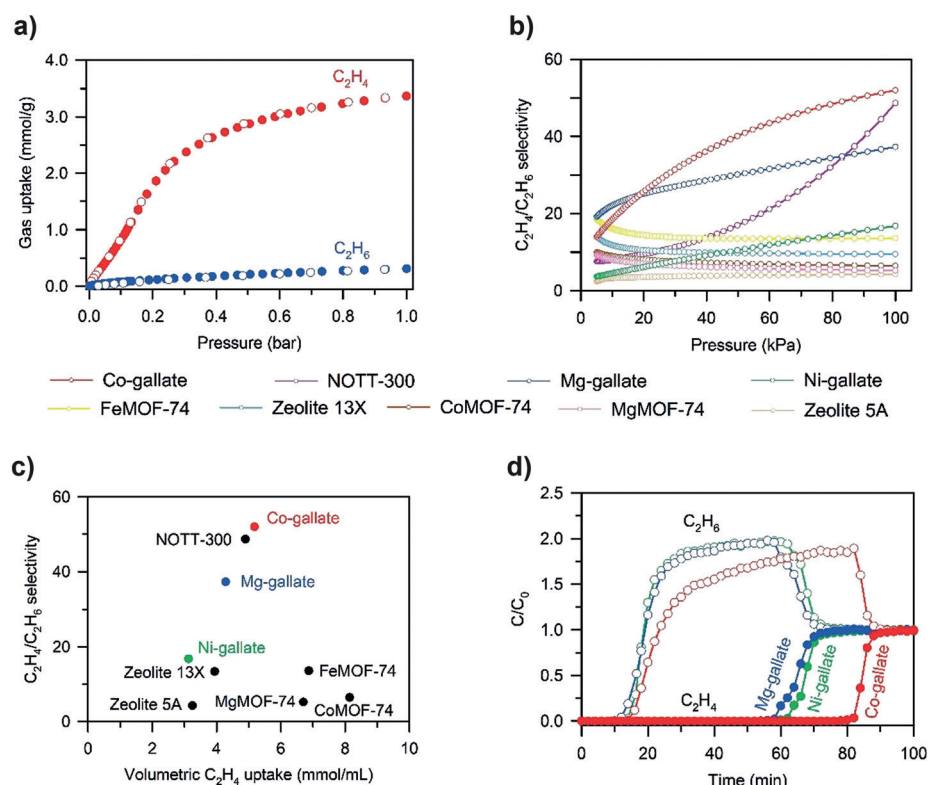
Figure 2. a) Single-component adsorption isotherms of C_2H_4 (red) and C_2H_6 (blue) in Co-gallate at 298 K in the pressure range of 0–1 bar. Empty symbols represent desorption data. b) Comparison of IAST selectivities for equimolar C_2H_4/C_2H_6 mixtures in M-gallate with other best-performing materials in the range of 0–1 bar. The adsorption isotherms were collected at 318 K for FeMOF-74,[10a] 298 K for M-gallate, MgMOF-74[9a] and zeolite 13X,[21] 296 K for CoMOF-74,[22] 293 K for NOTT-300,[23] and 283 K for zeolite 5A.[24] c) Comparison of C_2H_4/C_2H_6 adsorption selectivity and volumetric C_2H_4 uptake at 1 bar in M-gallate and other best-performing materials. d) Experimental breakthrough curves of M-gallate for the equimolar C_2H_4/C_2H_6 mixture at 273 K and 1 bar with a constant flow rate of 0.5 mL min^{-1}.
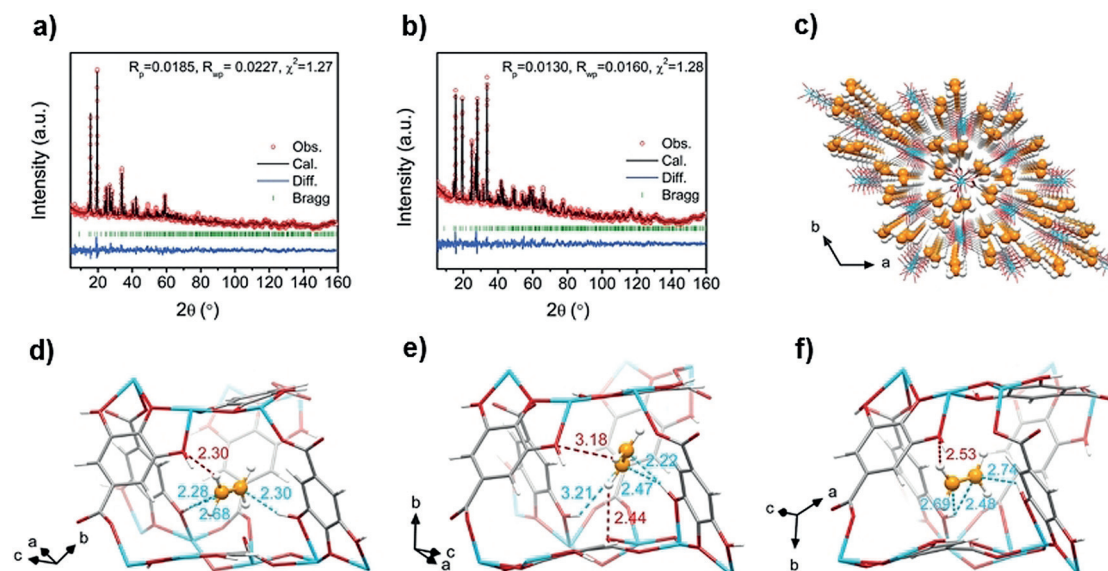
Figure 3. a),b) Rietveld refinements of the NPD data for a) bare Mg-gallate and b) C_2D_4-loaded Mg-gallate, both measured at 200 K. The ligand molecules and the C_2D_4 molecules were kept as rigid bodies during the refinement. Experimental (circles), calculated (line), and difference (line below observed and calculated) neutron powder diffraction profiles are shown. Vertical bars indicate the calculated positions of Bragg peaks. The goodness of fit data are shown in insets. c) Neutron diffraction crystal structure of Mg-gallate·0.485 C_2D_4 at 200 K from Rietveld analysis showing all C_2D_4 molecules are located in the branched channels. d)–f) Adsorption binding sites in Mg-gallate. d) Site I, e) Site II, and f) Site III. The C···H supramolecular interactions of C···H—O and C—D···O hydrogen-bonds are highlighted in cyan and red, respectively. Mg, C, O, H in Mg-gallate are represented by cyan, gray, red, and white, respectively; C and D in C_2D_4 are represented by orange and white, respectively.

metal sites (Supporting Information, Table S3) despite higher than NOTT-300 (16 kJ mol^{-1}). These adsorption results suggest M-gallate is a promising candidate for C_2H_4/C_2H_6 separation. To further understand the outstanding separation performance of M-gallate, the adsorption structure of C_2D_4 in Mg-gallate was established through high-resolution neutron powder diffraction (NPD) experiments (Figure 3 a,b). As shown in Figure 3 c and the Supporting Information, Figure S9, different from the water molecules residing in the *c*-axis straight channels (Supporting Information, Figure S10), all C_2D_4 molecules are located preferentially at the intersections of the straight and zigzag channels, most probably attributed to the larger molecule dimensions of C_2D_4 than H_2O, as well as the smaller aperture size of *c*-axis straight channels for hosting. Due to the slightly distorted trigonal lattice of activated Mg-gallate, the adsorbed C_2D_4 molecules belong to three crystallography sites, which differ only a little in terms of local pore environment (Figure 3 d-f; Supporting Information, Figure S11). Taking Site I (Figure 3 d) as an example, the C_2D_4 molecule is surrounded by a cycle composed of metal ions and two neighboring gallate ligands, and bound to the framework through cooperative supramolecular interactions between C(δ^-) of C_2D_4 and H(δ^+) from −OH of the two parallel gallate ligands (C···H—O = 2.28–2.68 Å). Furthermore, the side-on C—D···O hydrogen bonding interactions between C—D of C_2D_4 and the gallate ligand further strengthened the restraint against the C_2D_4 molecules. The bond length of the supramolecular interactions and hydrogen bonds had a similar but a very slight change at Site II and III (Figure 3 e,f) attributed to the slight distortion of the framework structure after dehydration (Supporting Information, Figure S3).

Among M-gallate, Mg-gallate not only keeps intermediate C_2H_4/C_2H_6 separation performance between Co- and Ni-gallate, but also is more thermally stable than Ni, Co-gallate, as evident by the TGA results (Supporting Information, Figure S12), arising from the higher hardness of Mg^{II}. Moreover, Mg^{II} salt is also cheaper and comparatively nontoxic compared with most transition metals.[25] Hence, we chose Mg-gallate to further investigate the industrial potential. Mg-gallate could be readily synthesized from gallic acid (ca. $10 kg^{-1}), which is produced on a massive scale from biomass, and the whole synthetic process is environmentally friendly without the use of organic solvents. Furthermore, the PXRD patterns and C_2H_4 uptake of Mg-gallate are still consistent with that of the as-synthesized sample even after being exposed in humid atmosphere (20 °C, and 75 % humidity) for 3 weeks (Supporting Information, Figures S13, S14), proving that Mg-gallate is highly stable against water vapor. Subsequently, multiple breakthrough tests revealed that Mg-gallate maintained its C_2H_4 uptake and complete molecular exclusion of C_2H_6 over 10 cycles (Supporting Information, Figure S15), illustrating the recyclability of Mg-gallate in the separation of the C_2H_4/C_2H_6 mixture. Besides, the excellent chemical and water stability of Mg-gallate was verified by unchanged PXRD patterns even after soaking in water and ethanol for 5 weeks (Supporting Information, Figure S16). Moreover, we investigated the feasibility of usage of Mg-gallate in industrial practice, and powder Mg-gallate was obtained by scale-up synthesis in the flask at ambient pressure. The PXRD patterns (Supporting Information, Figure S13) and adsorption isotherm for C_2H_4 (Supporting Information, Figure S17) exhibit no notable differences, indicating that the performance of efficient separation for

gas mixture would not differ from each other. Afterwards, millimeter-sized extrudates were shaped by addition of a binder material (Supporting Information, Figure S18), and the excellent separation performance for C_2H_4/C_2H_6 mixture was well retained (Supporting Information, Figures S19, S20). Therefore, Mg-gallate shows great potential in the practical separation of C_2H_4 and C_2H_6 in view of ready availability of ligand and easy preparation.

In summary, we demonstrated for the first time that a family of M-gallate (M = Ni, Mg, Co) MOFs are capable of selectively adsorbing ethylene while blocking ethane because of the perfect aperture dimension falling in the range between the minimum cross-section size of ethylene and that of ethane, affording benchmark high selectivity of ethylene over ethane. High ethylene uptake may also be realized due to high utilization efficiency of the quasi-discrete branched channels, where cooperative supramolecular interactions between ethylene and framework occurred. With several merits including readily available ligand, high stability against water vapor combined with the excellent maintenance of separation performance, M-gallate shows great potential in industrial practice, such as the pressure-swing adsorption process.

Conflict of interest

The authors declare no conflict of interest.

Keywords: adsorption separation · ethane · ethylene · metal–organic frameworks · purification

How to cite: *Angew. Chem. Int. Ed.* **2018**, *57*, 16020–16025
Angew. Chem. **2018**, *130*, 16252–16257

[1] a) R. B. Eldridge, *Ind. Eng. Chem. Res.* **1993**, *32*, 2208–2212; b) H. A. Wittcoff, B. G. Reuben, J. S. Plotkin, *Industrial organic chemicals*, Wiley, Hoboken, **2005**.

[2] D. S. Sholl, R. P. Lively, *Nature* **2016**, *532*, 435–437.

[3] R. T. Yang, *Adsorbents: fundamentals and applications*, Wiley, Hoboken, **2003**.

[4] K. Tanaka, A. Taguchi, J. Hao, H. Kita, K. Okamoto, *J. Membr. Sci.* **1996**, *121*, 197–207.

[5] T. A. Reine, R. B. Eldridge, *Ind. Eng. Chem. Res.* **2005**, *44*, 7505–7510.

[6] P. J. Bereciartua, Á. Cantín, A. Corma, J. L. Jordá, M. Palomino, F. Rey, S. Valencia, E. W. Corcoran, P. Kortunov, P. I. Ravikovitch, A. Burton, C. Yoon, Y. Wang, C. Paur, J. Guzman, A. R. Bishop, G. L. Casty, *Science* **2017**, *358*, 1068–1071.

[7] a) C. Gücüyener, J. van den Bergh, J. Gascon, F. Kapteijn, *J. Am. Chem. Soc.* **2010**, *132*, 17704–17706; b) J. Pires, M. L. Pinto, V. K. Saini, *ACS Appl. Mater. Interfaces* **2014**, *6*, 12093–12099; c) P. Q. Liao, W. X. Zhang, J. P. Zhang, X. M. Chen, *Nat. Commun.* **2015**, *6*, 8697.

[8] a) R. T. Yang, E. S. Kikkinides, *AIChE J.* **1995**, *41*, 509–517; b) S. Aguado, G. Bergeret, C. Daniel, D. Farrusseng, *J. Am. Chem. Soc.* **2012**, *134*, 14635–14637.

[9] a) Z. B. Bao, S. Alnemrat, L. Yu, I. Vasiliev, Q. L. Ren, X. Y. Lu, S. G. Deng, *Langmuir* **2011**, *27*, 13554–13562; b) B. Li, Y. Zhang, R. Krishna, K. Yao, Y. Han, Z. Wu, D. Ma, Z. Shi, T. Pham, B. Space, J. Liu, P. K. Thallapally, J. Liu, M. Chrzanowski, S. Ma, *J. Am. Chem. Soc.* **2014**, *136*, 8654–8660.

[10] a) E. D. Bloch, W. L. Queen, R. Krishna, J. M. Zadrozny, C. M. Brown, J. R. Long, *Science* **2012**, *335*, 1606–1610; b) S. J. Geier, J. A. Mason, E. D. Bloch, W. L. Queen, M. R. Hudson, C. M. Brown, J. R. Long, *Chem. Sci.* **2013**, *4*, 2054–2061.

[11] a) T. Fukushima, S. Horike, Y. Inubushi, K. Nakagawa, Y. Kubota, M. Takata, S. Kitagawa, *Angew. Chem. Int. Ed.* **2010**, *49*, 4820–4824; *Angew. Chem.* **2010**, *122*, 4930–4934; b) H. Deng, C. J. Doonan, H. Furukawa, R. B. Ferreira, J. Towne, C. B. Knobler, B. Wang, O. M. Yaghi, *Science* **2010**, *327*, 846–850; c) O. Shekhah, Y. Belmabkhout, Z. Chen, V. Guillerm, A. Cairns, K. Adil, M. Eddaoudi, *Nat. Commun.* **2014**, *5*, 4228–4235; d) J. Peng, H. Wang, D. H. Olson, Z. Li, J. Li, *Chem. Commun.* **2017**, *53*, 9332–9335; e) J. An, O. K. Farha, J. T. Hupp, E. Pohl, J. I. Yeh, N. L. Rosi, *Nat. Commun.* **2012**, *3*, 604–609; f) C.-T. He, Z.-M. Ye, Y.-T. Xu, D.-D. Zhou, H.-L. Zhou, D. Chen, J.-P. Zhang, X.-M. Chen, *Chem. Sci.* **2017**, *8*, 7560–7565.

[12] C. C. H. Lin, J. A. Sawada, L. Wu, T. Haastrup, S. M. Kuznicki, *J. Am. Chem. Soc.* **2009**, *131*, 609–614.

[13] a) B. Chen, N. W. Ockwig, A. R. Millward, D. S. Contreras, O. M. Yaghi, *Angew. Chem. Int. Ed.* **2005**, *44*, 4745–4749; *Angew. Chem.* **2005**, *117*, 4823–4827; b) X. Cui, K. Chen, H. Xing, Q. Yang, R. Krishna, Z. Bao, H. Wu, W. Zhou, X. Dong, Y. Han, *Science* **2016**, *353*, 141–144; c) P.-Q. Liao, N.-Y. Huang, W.-X. Zhang, J.-P. Zhang, X.-M. Chen, *Science* **2017**, *356*, 1193–1196; d) J. Li, J. Sculley, H. Zhou, *Chem. Rev.* **2012**, *112*, 869–932; e) Z. Chang, D.-H. Yang, J. Xu, T.-L. Hu, X.-H. Bu, *Adv. Mater.* **2015**, *27*, 5432–5441; f) B. Kesanli, Y. Cui, M. R. Smith, E. W. Bittner, B. C. Bockrath, W. Lin, *Angew. Chem. Int. Ed.* **2005**, *44*, 72–75; *Angew. Chem.* **2005**, *117*, 74–77; g) S.-T. Zheng, J. T. Bu, Y. Li, T. Wu, F. Zuo, P. Feng, X. Bu, *J. Am. Chem. Soc.* **2010**, *132*, 17062–17064; h) R. Vaidhyanathan, S. S. Iremonger, G. K. H. Shimizu, P. G. Boyd, S. Alavi, T. K. Woo, *Science* **2010**, *330*, 650–653; i) J. Wang, D. Xie, Z. Zhang, Q. Yang, H. Xing, Y. Yang, Q. Ren, Z. Bao, *AIChE J.* **2017**, *63*, 2165–2175.

[14] K. J. Chen, D. G. Madden, T. Pham, K. A. Forrest, A. Kumar, Q.-Y. Yang, W. Xue, B. Space, J. J. Perry, J.-P. Zhang, X.-M. Chen, M. J. Zaworotko, *Angew. Chem. Int. Ed.* **2016**, *55*, 10268–10272; *Angew. Chem.* **2016**, *128*, 10424–10428.

[15] R. B. Lin, L. Li, H. Wu, H. Arman, B. Li, R. G. Lin, W. Zhou, B. Chen, *J. Am. Chem. Soc.* **2017**, *139*, 8022–8028.

[16] A. Cadiau, K. Adil, P. M. Bhatt, Y. Belmabkhout, M. Eddaoudi, *Science* **2016**, *353*, 137–140.

[17] A. H. Assen, Y. Belmabkhout, K. Adil, P. M. Bhatt, D.-X. Xue, H. Jiang, M. Eddaoudi, *Angew. Chem. Int. Ed.* **2015**, *54*, 14353–14358; *Angew. Chem.* **2015**, *127*, 14561–14566.

[18] J.-R. Li, R. J. Kuppler, H.-C. Zhou, *Chem. Soc. Rev.* **2009**, *38*, 1477–1504.

[19] a) C. Reid, K. Thomas, *J. Phys. Chem. B* **2001**, *105*, 10619–10629; b) C. E. Webster, R. S. Drago, M. C. Zerner, *J. Am. Chem. Soc.* **1998**, *120*, 5509–5516.

[20] a) L. Cooper, T. Hidalgo, M. Gorman, T. Lozano-Fernandez, R. Simon-Vazquez, C. Olivier, N. Guillou, C. Serre, C. Martineau, F. Taulelle, D. Damasceno-Borges, G. Maurin, A. Gonzalez-Fernandez, P. Horcajada, T. Devic, *Chem. Commun.* **2015**, *51*,

5848–5851; b) R. K. Feller, A. K. Cheetham, *Solid State Sci.* **2006**, *8*, 1121–1125.

[21] S. H. Hyun, R. P. Danner, *J. Chem. Eng. Data* **1982**, *27*, 196–200.

[22] Y. He, R. Krishna, B. Chen, *Energy Environ. Sci.* **2012**, *5*, 9107–9120.

[23] S. Yang, A. J. Ramirez-Cuesta, R. Newby, V. Garcia-Sakai, P. Manuel, S. K. Callear, S. I. Campbell, C. C. Tang, M. Schroder, *Nat. Chem.* **2015**, *7*, 121–129.

[24] M. Mofarahi, S. M. Salehi, *Adsorption* **2013**, *19*, 101–110.

[25] B. Saccoccia, A. M. Bohnsack, N. W. Waggoner, K. H. Cho, J. S. Lee, D. Y. Hong, V. M. Lynch, J. S. Chang, S. M. Humphrey, *Angew. Chem. Int. Ed.* **2015**, *54*, 5394–5398; *Angew. Chem.* **2015**, *127*, 5484–5488.